ACS APPLIED MATERIALS & INTERFACES

Research Article

www.acsami.org

Fluorescent Organic Nanoparticles Based on Branched Small Molecule: Preparation and Ion Detection in Lithium-Ion Battery

Jinshan Wang, Xinjun Xu,* Leilei Shi, and Lidong Li*

State Key Lab for Advanced Metals and Materials, School of Materials Science and Engineering, University of Science and Technology Beijing, Beijing 100083, P. R. China

Supporting Information

ABSTRACT: Fluorescent organic nanoparticles (FONs) as a new class of nanomaterials can provide more advantages than molecule based probes. However, their applications in specific metal ion detection have rarely been exploited. We design and synthesize a branched small-molecule compound with triazole as a core and benzothiadiazole derivative as branches. By a facile reprecipitation method, nanoparticles (NPs) of this compound can be prepared in aqueous solutions, which can show high selectivity and sensitivity to Fe(III) ions based on fluorescence quenching. In addition, the fluorescence intensity of these NPs is resistant to pH changes in solutions. Such characters of this kind of NPs can be utilized in Fe^{3+} impurity detection in a promising cathode material ($LiFePO_4$) for lithium ion batteries. When exposed to Fe^{3+}, both the triazole and benzothiadiazole groups contribute to the fluorescence quenching of NPs, but the former one plays a more important role in Fe^{3+} impurity detection. The sensing mechanism has also been investigated which indicates that a Fe-organic complex formation may be responsible for such sensing behavior. Our findings demonstrate that specific metal ion detection can be realized by FONs and have extended the application field of FONs for chemical sensing in aqueous solutions.

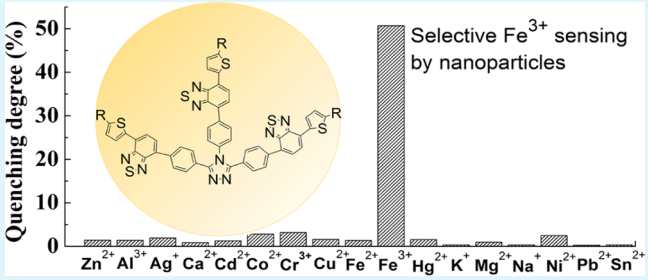

KEYWORDS: *fluorescence, organic nanoparticles, ion detection, lithium iron(II) phosphate, branched small molecule, lithium-ion battery*

INTRODUCTION

Fluorescence method as one of the most important methods to detect metal ions in environmental and biological systems has been widely applied and rapidly developed. Especially in recent years, lots of the conjugated polymers (CPs) were developed for specific ion sensing, such as Hg^{2+}, Fe^{2+}, Cu^{2+}, Pd^{2+}, Pb^{2+}, Ag^{+}, K^{+}, and Mg^{2+}.[1−9] The fluorescence method has obvious advantages in sensitivity, selectivity and real-time in situ detection.[10,11] However, most of these detections employ molecularly dispersed solutions that suffer from problems such as photobleaching, blinking, and intractable self-quenching.[12−16] By comparison, nanoparticles (NPs) of the fluorescent organic materials exhibit improved photostability and enhanced emission.[17−19] Currently, fluorescent organic nanoparticles (FONs) have been investigated in photocatalysis,[20] cell imaging,[21−24] and biosensing.[25,26] It is worth noting that FONs have good stability in aqueous solution, thus providing convenience for chemical and biological testing in aqueous solution.[27,28] Small-molecule FONs have their own advantages compared with CPs, including well-defined molecular structures, easier purification, amenability to large-scale production, and better batch-to-batch reproducibility.[29,30] However, there are rare reports on small-molecule FONs for metal ion detection.

Since the first report by Padhi in 1997,[31] lithium iron(II) phosphate ($LiFePO_4$) has been considered as a competitive candidate of cathode material for the next-generation green and sustainable lithium-ion battery system because of its long lifespan, abundant resources, low toxicity, and high thermal stability.[32−35] After years of development, besides its application in portable electronic devices, the olivine $LiFePO_4$ material optimized by carbon coating and nanotechnology also displays an excellent rate capability for powering electric vehicles and hybrid electric vehicles.[36] For preparation of $LiFePO_4$, Fe(III) raw materials such as $Fe(NO_3)_3$ and Fe_2O_3 were commonly used as the iron source,[37,38] which may leave untransformed Fe^{3+} matter as an impurity in the formed $LiFePO_4$. In addition, oxidation of Fe^{2+} into Fe^{3+} during the process of forming precursor $LiFePO_4$ glasses under high temperature for the fabrication of $LiFePO_4$ crystals is inevitable.[39] The presence of Fe^{3+} in $LiFePO_4$ cathode materials causes the self-discharge increase and specific capacitance decline, leading to degradation of the battery performance. So the content of Fe^{3+} is one of the most important parameters to evaluate the quality of $LiFePO_4$.

Received: February 1, 2013
Accepted: March 27, 2013
Published: March 27, 2013

dx.doi.org/10.1021/am4004396 | ACS Appl. Mater. Interfaces 2013, 5, 3392−3400

Currently, spectrophotometric methods are mostly used for the determination of Fe^{3+}, which need a metal complex formation reaction between Fe^{3+} and some chromogenic reagents. Although the spectrophotometric methods are simple and low-cost, their sensitivity is not high enough (the detection limit is usually in the range of 1×10^{-5} to 1×10^{-4} M).[40,41] In addition, the stability of these metal complexes can be affected by pH value and the composition of the buffers, and the measured results may also suffer from the interference from other ions.[42−44] Another promising way for Fe^{3+} determination is the fluoroionophore method. To date, some CPs and small-molecule probes have been developed for detection of Fe^{3+} using fluoroionophore method,[45−50] since Fe^{3+} is a fluorescence quencher due to its paramagnetic nature.[51] However, several obstacles limit the practical application of these molecular probes for realizing Fe^{3+} detection in $LiFePO_4$. First, many of probers can not avoid the interference of other metal ions like Cu^{2+} and Fe^{2+}.[52−55] Second, low sensitivity and low water solubility of many fluorescent sensors are still the challenges. Lastly, nonresistance to acid condition makes lots of fluorescent probes incompatible to $LiFePO_4$ because it must be dissolved in a strong acid during Fe^{3+} determination. Up to now, an effective method to detect the content of Fe^{3+} in $LiFePO_4$ is still absent.

In this work, we designed and synthesized a new type of small-molecule fluorescent material with a branched structure based on 3,4,5-triphenyl-4*H*-1,2,4-triazole (TAZ) as a core and 4-(5-hexylthiophen-2-yl)benzo[c][1,2,5]thiadiazole (BTTC6) as arms (referred to as TAZ-BTTC6). The combination of σ donor (nitrogen lone-pair electrons) and π receptor (highly electron deficient aromatic ring) makes triazoles a good ligand for Fe^{3+}.[56] Moreover, many C═N type nitrogen atoms in heteroatom-containing polymers have been reported to exhibit Fe^{3+} ion sensory properties, where N atom exhibits a variety of coordination modes.[57,58] So the combination of benzothiadiazole and triazole groups would act as an efficient chemosensor for Fe^{3+}. Our synthesis method is simple, and the compound can be easily prepared as nanoparticles in aqueous solution. In addition to this, fluorescence intensity of these NPs is resistant to pH changes in solutions. By utilizing this kind of FON as a chemosensor, Fe^{3+} ion detection in $LiFePO_4$ cathode materials has been achieved. The sensitivity and selectivity of TAZ-BTTC6 NPs for the detection of Fe^{3+} in the presence of other competing metal ions were established. Our work provides a high-sensitivity (with detection limit of 10^{-7} M), simple and convenient method for the utilization of small-molecule FONs in metal ion detection for the first time, which is especially useful for sensing the Fe^{3+} impurity in $LiFePO_4$.

EXPERIMENTAL SECTION

Materials and Measurements. Unless otherwise stated, the reagents used in our experiments were purchased from J&K Chemical or Sigma Aldrich Co. and were used without further purification. $LiFePO_4$/C composite was kindly provided by China Chaowei Power Co., Ltd. Tetrahydrofuran (THF) was distilled from Na/diphenylketone and *N*,*N*-dimethylformamide was dried by CaH_2. Other solvents were purchased from Beijing Chemical Works and used as received. Ultraviolet−visible (UV) absorption and photoluminescence (PL) emission spectra were measured on a Hitachi U-3900H spectrophotometer and a Hitachi F-7000 fluorescence spectrophotometer, respectively. The ^{1}H NMR and ^{13}C NMR spectra were recorded on 400 MHz AC Bruker spectrometer. Element analysis was conducted on a FLASH EA 1112 element analyzer. Mass spectra measurements were performed on a Bruker Daltonics BIFLEX III MALDI-TOF analyzer using MALDI mode. The size distributions of the NPs in aqueous solution were measured by the dynamic light scattering technique with a Malvern Zetasizer Nano ZS90. The morphology of the NPs was observed using an JEOL JSM-7401F high-resolution scanning electron microscope (HRSEM, accelerating voltage: 3.0 kV). The pH values of the solutions were measured by a pH meter.

Synthesis. *4-Bromo-N′-(4-bromobenzoyl)benzohydrazide (**1**).* At 0 °C, hydrazine monohydrate (0.75 g, 15 mmol) was slowly added to a mixture of triethylamine (2.75 g, 30 mmol) and 4-bromobenzoyl chloride (6.75 g, 30 mmol) in 30 mL of chloroform. The resulting mixture was stirred at room temperature for another 4 h. The solvent was then removed and the residual solid was washed with petroleum ether and deionized water twice to afford **1** (5.97g, 90% yield) as a white solid. ^{1}H NMR ($CDCl_3$, ppm): δ 7.87−7.85 (d, 4H), 7.77−7.73 (d, 4H), 7.66−7.64 (d, 2H). ^{13}C NMR ($CDCl_3$, ppm): δ 165.39, 132.09, 131.8, 130.05, 126.19.

*4-Bromo-N′-((4-bromophenyl)chloromethylene)-benzohydrazonoyl chloride (**2**).* Under argon atmosphere, the mixture of **1** (3.2 g, 8 mmol), phosphorus pentachloride (3.84 g 18 mmol) and 50 mL of toluene was stirred at 110 °C for 3 h. After removing of toluene, the solid was washed with deionized water and dried in vacuo and then recrystallized from ethanol to afford **2** (2.4 g, 72% yield) as a white powder. ^{1}H NMR ($CDCl_3$, ppm): δ 7.98−7.96 (d, 4H), 7.60−7.58(d, 4H). ^{13}C NMR ($CDCl_3$, ppm): δ 143.86, 132.49, 131.86, 129.98, 126.88.

3,4,5-Tris(4-bromophenyl)-4H-1,2,4-triazole (TAZBr). **2** (2.4 g, 5.5 mmol) and 4-bromoaniline (0.95 g, 5.5 mmol) were dissolved in 15 mL degassed *N*,*N*-dimethylformamide and stirred for 12 h at 120 °C under the argon atmosphere. An aqueous solution of HCl (10 mL, 2N) was added to the above mixture and stirred for an additional 30 min. The white precipitation was collected and washed with a plenty of deionized water, dried in vacuo. The residue was purified by column chromatography on silica gel using petrol ether:ethyl acetate as eluent yielding a white crystal (1.7 g, 58.2% yield). ^{1}H NMR ($CDCl_3$, ppm): δ 7.59−7.57 (d, 2H), 7.46−7.44 (d, 4H), 7.26−7.24 (d, 4H), 7.00−6.98 (d,2H). ^{13}C NMR ($CDCl_3$, ppm): 154.08, 134.18, 133.38, 132.17, 131.13, 129.80, 126.27, 124.00.

*2-Bromo-5-hexylthiophene (**3**).* A solution of 2,5-dibromothiophene (7.5 g, 31 mmol) in THF (30 mL) was cooled to −78 °C under argon, and n-BuLi (1.6 M n-hexane solution, 21.3 mL, 34.1 mmol) was added dropwise. The reaction was lasted for 1 h under stirring at −78 °C. Then, 1-bromohexane (6.6 mL, 46.5 mmol) was added and the mixture was stirred for additional 2 h at −78 °C. The reacted solution was allowed to warm to room temperature and was stirred overnight. To this solution, H_2O (30 mL) was added and then extracted with chloroform (3 × 50 mL). The organic layer was dried over anhydrous sodium sulfate and the solvent was removed in vacuo. The crude oil was purified via a short column chromatography on silica gel using petroleum ether as eluent, yielding a clear yellow oily liquid (7.3 g, 96% yield). The product was directly used in the next reaction.

*2-(5-Hexylthiophen-2-yl)-4,4,5,5-tetramethyl-1,3,2-dioxaborolane (**4**).* n-BuLi (1.6 M n-hexane solution, 18 mL, 17.04 mmol) was added dropwise to a solution of **3** (6 g, 14.2 mmol) in dry THF (20 mL) at −78 °C under the argon atmosphere. The reaction solution was stirred for 1 h at −78 °C. Then, 2-isopropoxy-4,4,5,5-tetramethyl-1,3,2-dioxaborolane (6 mL, 17.04 mmol) was added and the reaction was kept for additional 2 h at −78 °C. After that, the reaction solution was allowed to warm to room temperature overnight. To this solution, H_2O (30 mL) was added to quench the reaction, and then the mixture was extracted with chloroform (3 × 50 mL). The organic layer was dried over anhydrous sodium sulfate and the solvent was removed in vacuo. The crude oil was purified by column chromatography on silica gel using petrol ether:ethyl acetate as eluent yielding clear yellow oil (4.0 g, 95% yield). ^{1}H NMR ($CDCl_3$, ppm): δ 7.46 (d, 1H), 6.85(d, 1H), 2.83(m, 2H), 1.65 (m, 2H), 1.32−1.23 (m, 18H) 0.87(t, 3H).

*4-bromo-7-(5-hexylthiophen-2-yl)benzo[c][1,2,5]thiadiazole(**5**).* 4,7-Dibromobenzo[c][1,2,5]thiadiazole (2 g, 6.8 mmol), **4** (2 g, 6.8 mmol), degassed toluene (12 mL) and degassed Na_2CO_3 (2 M aqueous solution, 5 mL) was added to a 50 mL Schlenk flask and the solution was degassed for 10 min. $Pd(PPh_3)_4$ (40 mg, 0.34 mmol) was

Scheme 1. Synthesis Route of TAZ-BTTC6

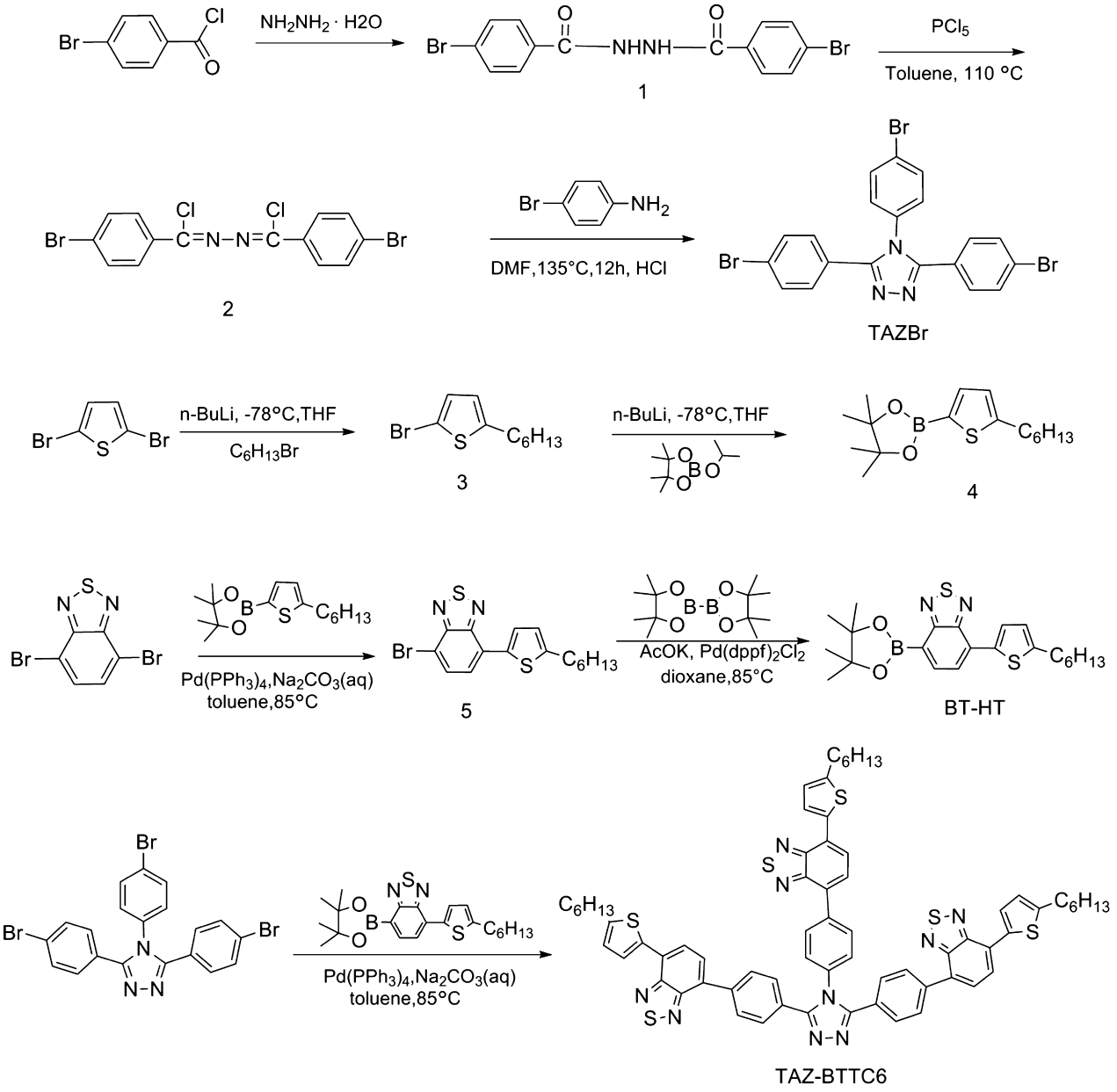

added to the solution and the mixture was stirred for 10 min under argon. The mixture was heated to 85 °C and kept for 3 h. Then the reaction was quenched with water (20 mL) and the mixture was extracted with chloroform (3 × 30 mL). The organic layer was dried over anhydrous sodium sulfate and the solution was removed. The crude was get through a short column chromatography yielding a yellow solid (1.52 g, 58.8% yield), which was used directly for the next step.

4-(5-Hexylthiophen-2-yl)-7-(4,4,5,5-tetramethyl-1,3,2-dioxaborolan-2-yl)benzo[c][1,2,5]thiadiazole (BT-HT). Bis(pinacolato)diboron (5 g, 20 mmol), **5** (1.52 g, 4 mmol), potassium acetate (2 g, 20 mmol) and $Pd(dppf)Cl_2$ (146 mg, 0.2 mmol) were added to dioxane (10 mL) in a 25 mL Schlenk flask. The mixture was degassed with argon gas for 30 min, and then heated to 85 °C for 24 h. The reaction was quenched with water (10 mL) and the mixture was extracted with chloroform (3 × 30 mL). The organic layer was dried over anhydrous sodium sulfate and the solvent was removed. The crude was purified by column chromatography on silica gel using petrol ether:ethyl acetate as eluent yielding a sticky solid (1.22 g, 71% yield). ^{1}H NMR ($CDCl_3$, ppm): δ 8.18−8.16 (d, 1H), 8.04−8.03 (d,1H), 7.88−7.86 (d, 2H), 6.91−6.90 (d, 1H), 2.93−2.88 (t, 2H), 1.74−1.71 (m, 2H), 1.41−1.39 (s, 12H) 1.23 (m, 6H), 0.87 (t, 3H).

Synthesis of TAZ-BTTC6. TAZBr (280 mg, 0.52 mmol), BT-HT (1.22 g, 2.85 mmol), $Pd(pph_3)_4$ (164 mg, 0.13 mmol) and tetrabutyl ammonium bromide (40 mg, 0.13 mmol) were added to a 25 mL Schlenk flask. After purging with argon gas for 10 min, degassed toluene (12 mL) and degassed Na_2CO_3 (2 M in aqueous solution, 5 mL) was added to the above mixture. Then the solution was subjected to vacuum/argon refill cycles for three times and heated to 85 °C for 42 h under argon atmosphere. The reaction solution was quenched by water (10 mL) and extracted with chloroform (3 × 30 mL). The organic layer was washed with brine (3 × 50 mL) and dried with Na_2SO_4. Then, the solvent was removed in vacuo and the residual was purified by column chromatography on silica gel using dichloromethane:ethyl acetate as eluent yielding a red brown solid (400 mg, 64% yield). ^{1}H NMR ($CDCl_3$, ppm): δ 8.18−8.16 (t, 3H), 7.97−7.91(m, 6H), 7.84−7.82 (d, 1H), 7.79−7.77 (d, 2H), 7.69−7.64 (m, 6H), 7.49 (m, 1H), 7.41−7.39 (d, 2H), 6.87−6.84 (m, 3H), 1.73−1.72 (m, 6H), 1.43−1.22 (m, 18H), 0.96−0.88 (m, 9H). ^{13}C NMR ($CDCl_3$, ppm): δ 154.66, 153.72, 153.59, 152.78, 152.73, 148.63, 148.57, 148.28, 148.22,

dx.doi.org/10.1021/am4004396 | ACS Appl. Mater. Interfaces 2013, 5, 3392−3400

138.76, 138.51, 136.55, 136.38, 130.77, 130.65, 129.64, 128.87, 128.75, 128.66, 128.39, 128.19, 128.11, 127.89, 127.33, 126.60, 125.37, 125.26, 124.89, 124.74, 33.70, 31.57, 30.31, 29.98, 28.82, 24.87, 22.57, 22.23, 14.05, 13.80. MS (MALDI-TOF) m/z: M^+ calcd for $C_{68}H_{63}N_9S_6$, 1198.68; found, 1198.6. EA calcd for $C_{68}H_{63}N_9S_6$: C 68.14, H 5.30, N 10.52; found: C 67.44, H 5.58, N 10.23.

Preparation of TAZ-BTTC6 NPs, BT-HT NPs and TAZBr Agglomeration-Suspended Solutions. TAZ-BTTC6 and BT-HT NPs were fabricated through a reprecipitation method.[59] Briefly, TAZ-BTTC6 and BT-HT were dissolved in THF to form molecularly dispersed solution with a concentration of 2.0 mg/mL, respectively. Then 0.25 mL of such a solution was rapidly injected into 10 mL of deionized water (18.3 MΩ) at 50 °C under ultrasonication. The resulting solution was ultrasonicated for 10 min followed by filtration with 0.22 μm poly(tetrafluoroethylene) filters. The obtained concentration of the TAZ-BTTC6 and BT-HT NP solution was 4.1×10^{-5} and 1.1×10^{-4} M, respectively. Then, they were diluted to 4.1×10^{-7} and 5.1×10^{-6} M, respectively, when used for measurements. TAZBr was dissolved in THF to form molecularly dispersed solution with a low concentration of 0.6 mg/mL due to its weak solubility. As for TAZBr, we tried to prepare the NPs solution following the same procedure as described above, but only an agglomeration-suspended solution can be gained (water:THF = 40:1 (v/v)) . The obtained concentration of the suspension solution was 2.7×10^{-5} M. Then it was diluted to 2.7×10^{-6} M when used for measurements..

Pretreatment of Lithium Iron(II) Phosphate. To get pure $LiFePO_4$ without Fe^{3+} impurity, pretreatment to the $LiFePO_4$/C composite was performed. Under argon atmosphere, 0.1000 g $LiFePO_4$/C composite material was added to an HCl solution (11 mL, 1.1 M), then the mixture was kept at 85 °C for 20 min to make sure $LiFePO_4$ was completely dissolved. After cooling, the mixture was filtered to remove the carbon black (0.0200g) and the filtrate was transferred to a 1000 mL volumetric flask. Then, stannous chloride (2.5×10^{-4} mol) was added to the 1000 mL volumetric flask based on the content of $LiFePO_4$ (the effective content of $Fe^{2+} < 5.0 \times 10^{-4}$ mol), and the mixture was maintained for 20 min at 80 °C under argon atmosphere to make sure Fe^{3+} ions were completely reduced to Fe^{2+}. In order to avoid the subsequently artificially introduced iron(III) matter being reduced, Cu^{2+} ions (5×10^{-4} mol, stannous ion were oxidized exactly) were introduced to remove excess stannous ions. Finally, the mixture solution was set to the volume of 1000 mL and cooled down to room temperature. The final pH value of the solution was 2.55. This solution was stored under the Ar atmosphere. Before the PL measurement, 1.98 mL of such solution in a cuvette was bubbled with argon to remove the air. Then, 20 mL of $FeCl_3$ aqueous solution was added to get the desired solution with different concentration of Fe^{3+}.

RESULTS AND DISCUSSION

Synthesis and Characterization of TAZ-BTTC6. The synthetic route is shown in Scheme 1. TAZ-BTTC6 was synthesized by the Suzuki coupling reaction of TAZBr and BT-HT. The intermediate compound TAZBr was prepared from 4-bromobenzoyl chloride as a starting material by reacting consecutively with hydrazine hydrate, phosphorus pentachloride and 4-bromoaniline. Compounds **4** and **5** and BT-HT were synthesized according the reported procedures.[60,61] TAZ-BTTC6 can be readily solved in common organic solvents such as chloroform, THF, and *o*-dichlorobenzene. TAZ-BTTC6 was fully characterized by ^{1}H NMR, ^{13}C NMR, matrix-assisted laser desorption ionization time-of-flight (MALDI-TOF) mass spectra (MS) (see the Supporting Information, Figure S1), and elemental analysis (EA). This compound shows good thermal stability with decomposition temperature of 427 °C and glass transition temperature of 237 °C (see Figure S2 in the Supporting Information).

Figure 1a shows the normalized UV absorption spectra and PL emission spectra of TAZ-BTTC6 in dilute THF solution

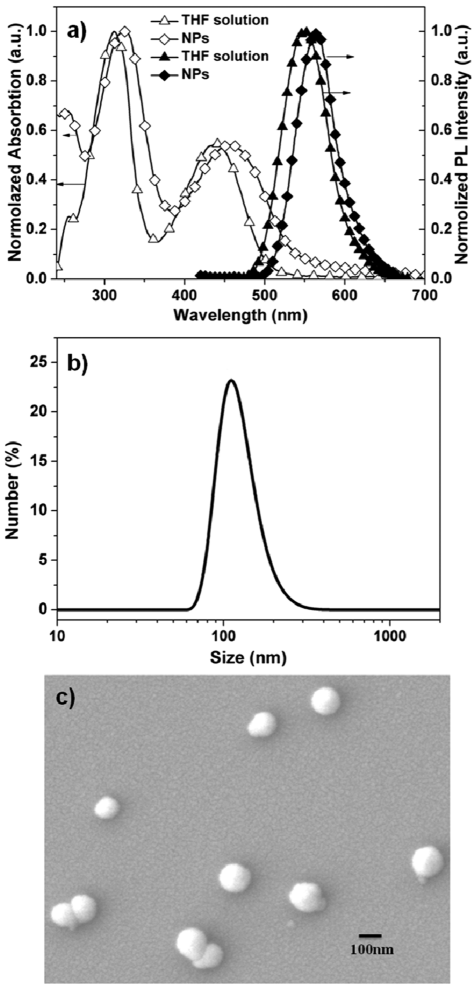

Figure 1. (a) Normalized UV absorption and PL emission spectra of TAZ-BTTC6 in dilute THF and NP aqueous solutions. (b) Size (diameter) distribution of TAZ-BTTC6 NPs in aqueous solution. (c) SEM images of TAZ-BTTC6 NPs morphology on the surface of silicon substrate.

and in NP aqueous solution. TAZ-BTTC6 in THF solution exhibits two strong absorption peaks at 312 and 439 nm. The absorption peaks of TAZ−BTTC6 NPs are red-shifted by 11 and 16 nm, respectively, relative to the molecularly dispersed state due to the stacking of molecules in NPs. The PL emission peak of TAZ-BTTC6 is located at 549 nm in THF solution, while it is red-shifted to 565 nm in NPs aqueous solution. The optic band gap of TAZ-BTTC6 estimated from the UV absorption edge of its dilute THF solution is 2.31 eV. Figure 1b shows the size distribution of TAZ-BTTC6 NPs in aqueous solution. TAZ-BTTC6 NPs have a number mean particle size of 125 nm and a Z-average of 175 nm (with a polydispersity index of 0.217, the calculations for these parameters are defined in the ISO standard document 13321:1996 E). In addition, they exhibit a zeta potential of −26.1 mV which is high enough to enable the NPs to be stabilized by static repulsion and not to be flocculated even after months of storage. Figure 1c shows the morphology of TAZ-BTTC6 NPs on the surface of silicon substrate characterized by HRSEM. From the image we can see, TAZ-BTTC6 NPs are nearly sphere-shaped with an average

diameter about 140 nm. The underlying small grains are composed of platinum which is used to enhance the conductivity of TAZ-BTTC6 NPs film. The intermediate BT-HT can also form NPs in aqueous solution whose size distribution is shown in Figure S3 (Supporting Information), whereas the intermediate TAZBr can not do and only an agglomeration-suspended solution can be obtained. The normalized UV and PL spectra of the TAZBr and BT-HT in THF solution and in the agglomeration/NP aqueous solutions are also examined (Supporting Information, Figure S4). TAZBr shows both UV absorption and PL emission peaks in the ultraviolet region, whereas BT-HT shows PL emission peak in the visible light region with green color.

Selective Metal Ion Sensing by TAZ-BTTC6 NPs. To study the ion sensing properties of TAZ−BTTC6 NPs, we investigated nearly 20 various metal ions including Al^{3+}, Ca^{2+}, Cd^{2+}, Co^{2+}, Cr^{3+}, Cu^{2+}, Fe^{2+}, Fe^{3+}, Hg^{2+}, K^{+}, Mg^{2+}, Na^{+}, Ni^{2+}, Pb^{2+}, Zn^{2+}, Ag^{+}, and Sn^{2+} under identical conditions. The PL emission spectra were obtained in aqueous solution with a pH value of 3.0. Figure 2a shows the quenching degrees (defined as $1-I/I_0$, where I_0 and I stands for the fluorescence intensity of NPs without and with ions addition, respectively) of TAZ-BTTC6 NP aqueous solutions (4.1×10^{-7} M) in the presence of each kind of ion (1×10^{-5} M). TAZ-BTTC6 NPs show a great response and good selectivity to Fe^{3+}. By contrast, the PL quenching degrees were not significant when Al^{3+}, Ca^{2+}, Cd^{2+}, Co^{2+}, Cr^{3+}, Cu^{2+}, Fe^{2+}, Hg^{2+}, K^{+}, Mg^{2+}, Na^{+}, Ni^{2+}, Pb^{2+}, Zn^{2+}, Ag^{+}, and Sn^{2+} were added into the NP solution. Especially, the quenching effect of K^{+}, Na^{+}, Pb^{2+}, and Sn^{2+} to PL intensity can be ignored. Except Fe^{3+}, the highest quenching degree only reaches 3.2%, which is the case of introducing Cr^{3+} ion (1×10^{-5} M). Nevertheless, the quenching degree in the presence of Fe^{3+} reaches to 51% under identical conditions. This value is 16−180 folds higher than other metal ions.

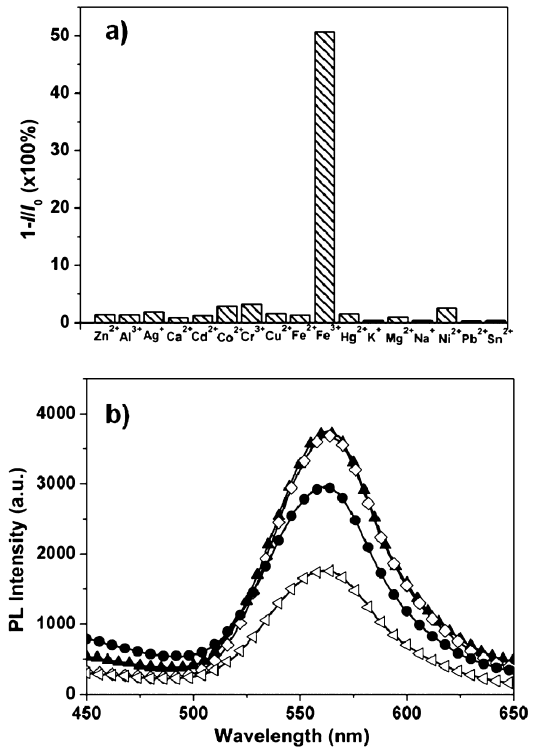

Figure 2. (a) PL quenching degrees ($1 - I/I_0$) of TAZ-BTTC6 NPs ([TAZ-BTTC6] = 4.1×10^{-7} mol L^{-1}) in response to each kind of metal ion (whose concentration is 1×10^{-5} mol L^{-1}). (b) PL spectra of TAZ-BTTC6 NP aqueous solution only (filled triangles), NPs with mixed metal ions except Fe^{3+} (see the main text for what metal ions being involved, the concentration of each kind of metal ion is 1×10^{-5} mol L^{-1}) (open diamonds), NPs with mixed metal ions including 1×10^{-6} mol L^{-1} Fe^{3+} (filled circles), and NPs with mixed metal ions including 1×10^{-5} mol L^{-1} Fe^{3+} (open triangles). All these solutions have the same TAZ-BTTC6 concentration of 4.1×10^{-7} mol L^{-1} and the same pH value of 3.0.

To further confirm the selectivity for Fe^{3+}, PL intensity of TAZ-BTTC6 NP solution with mixed metal ions was also studied. As shown in Figure 2b, the PL intensity of NP solution with the mixed metal ions (including Al^{3+}, Ca^{2+}, Cd^{2+}, Co^{2+}, Cr^{3+}, Cu^{2+}, Fe^{2+}, Hg^{2+}, K^{+}, Mg^{2+}, Na^{+}, Ni^{2+}, Pb^{2+}, Zn^{2+}, Ag^{+}, and Sn^{2+} with the metal ion concentration of 1×10^{-5} M for each kind) has only slightly reduced relative to that without metal ions addition. However, when Fe^{3+} was introduced into the system containing the mixed metal ions, the PL intensity causes a quenching degree of 17.7% even if the Fe^{3+} concentration is as low as 1×10^{-6} M. Furthermore, the PL quenching degree reaches 53.2% when Fe^{3+} concentration is 1×10^{-5} M.

This result indicates that TAZ-BTTC6 NPs can exhibit excellent selectivity for Fe^{3+}. To exclude the influence of pH value on the PL quenching of NPs, the PL spectra of TAZ-BTTC6 NP aqueous solutions under various pH values were tested and only slight changes were found during a wide pH range (1−11) (see Figure S5 in the Supporting Information).

Fe(III) Ion Detection in $LiFePO_4$. To extend the application of TAZ-BTTC6 NPs for Fe^{3+} detection in more important areas, $LiFePO_4$ which is a very promising cathode material in lithium-ion batteries has been selected to be an analyte. Figure 3a shows the PL spectra of TAZ-BTTC6 NPs in $LiFePO_4$ solution (TAZ-BTTC6: 4.1×10^{-7} M, $LiFePO_4$: 5×10^{-4} M) in the presence of Fe^{3+} with different concentrations. When the concentration of Fe^{3+} in the aqueous solution changed from 1×10^{-7} to 4×10^{-4} M, the PL intensity of TAZ-BTTC6 NPs was remarkably quenched. The quenching of TAZ-BTTC6 NPs PL intensity shows a nearly linear curvature at relatively low Fe^{3+} concentrations ($\leq 8 \times 10^{-6}$ M), as shown in Figure 3b. The quenching efficiency ($I_0/I-1$) and Fe^{3+} concentration conform to Stern−Volmer relationship (eq 1), where I_0 is the fluorescence intensity without addition of quencher, I is the fluorescence intensity in the presence of quencher with concentration [Q], and K_{SV} is the Stern−Volmer constant.

$$I_0/I - 1 = K_{sv}[Q] \quad (1)$$

When the concentration of Fe^{3+} is in the range of 1×10^{-7} to 8×10^{-6} M, the Stern−Volmer constant $K_{sv(TAZ\text{-}BTTC6)}$ is 6.1×10^4 M^{-1}. However, if the Fe^{3+} concentration is higher ($>1 \times 10^{-5}$ M), the linear relationship is not met (see Figure S6 in the Supporting Information). The change of PL intensity of TAZ-BTTC6 NPs in $FeLiPO_4$ solution versus Fe^{3+} concentration with a wide range of 1×10^{-7} to 4×10^{-4} M is shown in Figure 3c. As can be seen, the PL intensity decreases quickly in the low concentration region of Fe^{3+} ($<1 \times 10^{-5}$ M) and slowly in the high concentration region ($>1 \times 10^{-5}$ M).

Sensing Mechanism of TAZ-BTTC6 NPs. To further investigate which segment in TAZ-BTTC6 molecule plays a role in Fe^{3+} detection, the interactions of intermediates TAZBr and BT-HT with Fe^{3+} were studied by measuring the change of PL intensity of TAZBr suspension and BT-HT NP aqueous

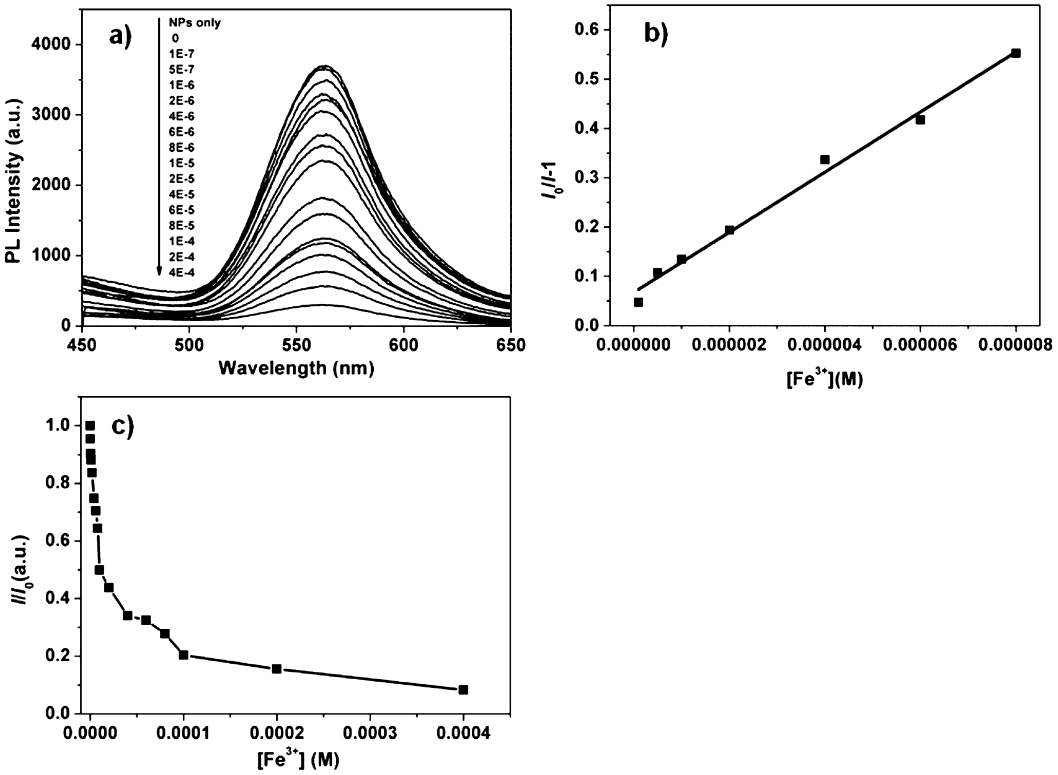

Figure 3. (a) PL spectra of TAZ-BTTC6 NPs in blank aqueous solution and in $LiFePO_4$ (5×10^{-4} mol L^{-1}) aqueous solution with different Fe^{3+} impurity concentrations ($0 - 4 \times 10^{-4}$ mol L^{-1}). The excitation wavelength is fixed at 280 nm. All these solutions have the same TAZ-BTTC6 concentration of 4.1×10^{-7} mol L^{-1}. (b) PL quenching efficiencies ($I_0/I-1$) of TAZ-BTTC6 NPs versus Fe^{3+} concentration in the low concentration region ($1 \times 10^{-7} - 8 \times 10^{-6}$ mol L^{-1}). (c) The change of PL intensity of TAZ-BTTC6 NP aqueous solution (4.1×10^{-7} mol L^{-1}) versus Fe^{3+} concentration in a wide range of 1×10^{-7} to 4×10^{-4} mol L^{-1}.

solutions (pH = 3) with Fe^{3+} addition. When Fe^{3+} was introduced into the solution ($[Fe^{3+}] = 1 \times 10^{-5}$ M), the fluorescence intensity of TAZBr suspension solution was quenched by 47% (as show in Figure 4a), while that of BT-HT NPs was quenched by 16% (see Figure 4b). This result implies that the both parts (TAZ and BTTC6) of TAZ-BTTC6 molecule have the sensing ability for Fe^{3+}, and the TAZ group shows higher sensitivity to Fe^{3+} than BTTC6 group. It should be noted that TAZ-BTTC6 NPs show a decrease in the PL intensity by 52% under the same condition, as shown in Figure 3c, which is larger than each of the individual part. It means that the TAZ-BTTC6 molecule has an amplification effect to the PL quenching caused by Fe^{3+}. The quenching effect might be attributed to the formation of complexes between Fe^{3+} and TAZ-BTTC6 when Fe^{3+} ions were introduced into the TAZ-BTTC6 NP aqueous solution. Because the mono-1,2,4-triazole ligands have many coordination modes,[62,63] they were reported to form complexes easily with Fe^{3+}.[64] As a result, we speculate that triazole group has a stronger affinity for Fe^{3+} compared with benzothiadiazole. Thus, the Fe^{3+} ions first interact with the TAZ group to form complex at a low Fe^{3+} concentration and a good linear relationship between the amount of Fe(III)-TAZ-BTTC6 complex and $[Fe^{3+}]$ can be found.

In order to verify the above hypothesis, the relationship between PL quenching efficiency of TAZBr suspension solution and $[Fe^{3+}]$ was studied, as shown in c and d in Figure 4. A linear relationship is found, which is similar as what TAZ-BTTC6 NPs have exhibited in the low concentration region of Fe^{3+}. From Figure 4d we can deduce the $K_{sv(TAZBr)}$ value is 6.3 $\times 10^4$ M^{-1}, which coincides with $K_{sv(TAZ\text{-}BTTC6)}$. It is well-known that K_{sv} is a constant to estimate the binding affinity of the quencher to the fluorophore.[1,65] The larger K_{sv} is, the higher the sensitivity of the fluorophore toward quencher is.[5] The measured $K_{sv(TAZ\text{-}BTTC6)}$ (6.1×10^4 M^{-1}) is large enough, which indicates a complex may be formed between TAZ-BTTC6 NPs and Fe^{3+}.

The complexation was verified by comparison of the ^1H NMR spectra of TAZ-BTTC6 with and without Fe^{3+} addition in solution, as shown in Figure 5. After introduction of 1 equivalent of Fe^{3+} to TAZ-BTTC6, the signals in the ^1H NMR spectrum turned to be weaker and broader in the downfield at 7.94 (hydrogens in benzothiadiazole) and 7.45 (hydrogens in thiophene) ppm. Meanwhile, the signals of 8.16, 7.79, and 7.67 (hydrogens in benzene close to triazole) ppm disappeared. The most possible reason to explain this phenomenon is the complex formation between Fe^{3+} and triazole group in TAZ-BTTC6. Due to the presence of paramagnetic iron, a partially reversed magnetic field is generated around the triazole group. The reversed magnetic field shields the signal generated by the NMR spectrometer, leading to an increased relaxation time and causing the hydrogen signals to be broader and even disappeared. This may explain why part of the hydrogen signals of benzene ring in downfield (7.4−8.2 ppm) disappeared and the hydrogen signals of alkyl chain in upfield were not affected. To further prove the hypothesis of complexation of Fe^{3+} to the triazole unit in TAZ-BTTC6 molecule, ^1H NMR spectra of TAZBr and BT-HT in solution with and without Fe^{3+} addition have also been investigated (Figure 5). It can be seen that TAZBr exhibits the similar phenomenon as TAZ-BTTC6, which shows only a broad

dx.doi.org/10.1021/am4004396 | ACS Appl. Mater. Interfaces 2013, 5, 3392−3400

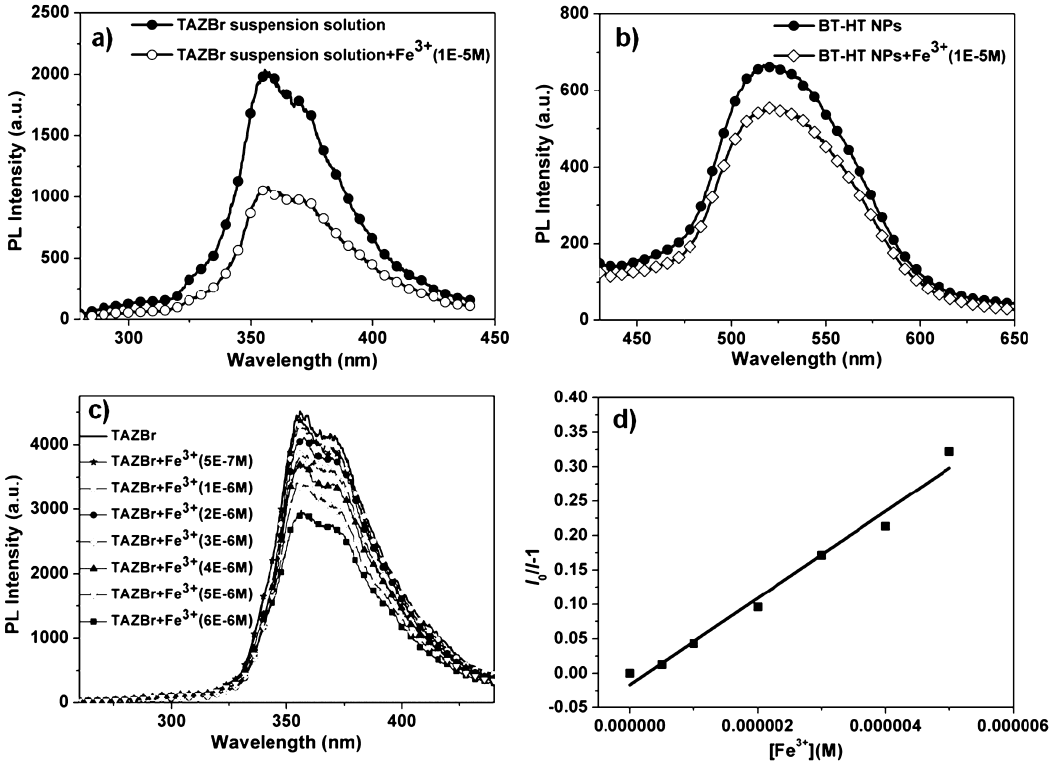

Figure 4. (a) PL spectra of TAZBr suspension solution (2.7×10^{-6} mol L^{-1}) and upon adding Fe^{3+} (1×10^{-5} mol L^{-1}). b) PL spectra of BT-HT NP aqueous solution (5.1×10^{-6} mol L^{-1}) and upon adding Fe^{3+} (1×10^{-5} mol L^{-1}). (c) Fe^{3+} concentration dependent variations in the PL intensity of TAZBr suspension solution. d) PL quenching efficiency ($I_0/I-1$) of TAZBr suspension solution versus Fe^{3+} concentration (in the range of 5×10^{-7} to 5×10^{-6} mol L^{-1}).

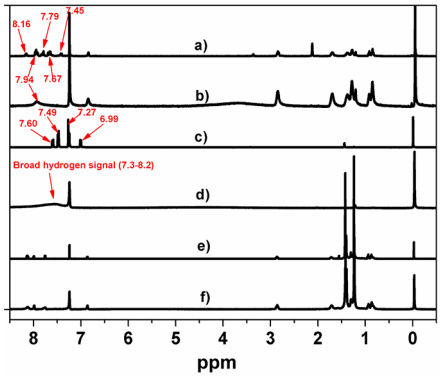

Figure 5. ^{1}H NMR spectra of TAZ-BTTC6, TAZBr and BT-HT in $CDCl_3$ (a, c, e) in the absence of Fe^{3+}, and (b, d, f) in $CDCl_3$:CD_3OD (30:1, v/v) in the presence of 1 equivalent of Fe^{3+} , respectively.

hydrogen signal in downfield (7.3−8.2 ppm) combining with disappearance of some hydrogen signals. By contrast, BT-HT does not show any obvious change in its ^{1}H NMR spectrum after the addition of Fe^{3+}.

From the above analysis, it can be reasonably deduced that the PL quenching effect of TAZ-BTTC6 NPs when exposed to Fe^{3+} is mainly resulted from the complexation between Fe^{3+} and the triazole unit. It is well know that the metal complexation usually obeys stoichiometry. As a result, a linear relationship exists between the PL quenching degree of TAZ-BTTC6 NPs and the concentration of Fe^{3+} ($<1 \times 10^{-5}$ M). When the concentration of Fe^{3+} is high ($>1 \times 10^{-5}$ M), besides its preferential complexation with the TAZ group in TAZ-BTTC6 molecule, the remaining Fe^{3+} can interact with the BTTC6 branches. Different with TAZ group, the BTTC6 group does not show complexation with Fe^{3+} and the interaction between them may be partial charge transfer. Due to the weaker affinity of BTTC6 to Fe^{3+}, in the high concentration region the PL intensity of TAZ-BTTC6 NPs reduces slowly and the quenching degree is not linear with the concentration of Fe^{3+}.

CONCLUSIONS

A new type of branched small molecule TAZ-BTTC6 was designed and synthesized. Through a facile reprecipitation method, FONs made from TAZ-BTTC6 can be prepared in aqueous solutions with high stability. TAZ-BTTC6 NPs show high sensitivity and excellent selectivity for Fe^{3+} among nearly twenty kinds of metal ions. By virtue of these advantages and their resistance to strong acid, TAZ-BTTC6 NPs have been utilized to act as fluorescent probes for Fe^{3+} impurity detection in $LiFePO_4$ which is a promising cathode material for lithium ion batteries. The PL intensity of TAZ-BTTC6 NPs does not show quenching in pure $LiFePO_4$ dissolved in acid solution, but it is quenched dramatically when Fe^{3+} impurity is existed. The detection limit for Fe^{3+} can be as low as 1×10^{-7} M. The fluorescence quenching is attributed to the formation of Fe^{3+}-TAZ-BTTC6 complex by binding of Fe^{3+} to the TAZ unit in TAZ-BTTC6 molecule. To the best of our knowledge, this is the first report about using small-molecule FONs as the selective metal-ion chemosensors. Since FONs have many advantages over molecularly dispersed solutions, our results may be of great help for extending the application of fluorescent small-molecule materials, which are usually non-

dx.doi.org/10.1021/am4004396 | ACS Appl. Mater. Interfaces 2013, 5, 3392−3400

water-soluble, to the field of chemical and biological sensing in aqueous solutions.

■ ASSOCIATED CONTENT

Supporting Information

MALDI-TOF MS spectra and thermal analysis of TAZ-BTTC6, impact of PH values, size distribution of BT-HT NPs, and spectra of TAZBr and BT-HT. This material is available free of charge via the Internet at http://pubs.acs.org.

■ AUTHOR INFORMATION

Corresponding Author

*E-mail: xuxj@mater.ustb.edu.cn (X.X.); lidong@mater.ustb.edu.cn (L.L.).

Notes

The authors declare no competing financial interest.

■ ACKNOWLEDGMENTS

This work is supported by the National Natural Science Foundation of China (51273020, 90923015), the Fundamental Research Funds for the Central Universities, the Program for Changjiang Scholars and Innovative Research Team in University and the State Key Lab for Advanced Metals and Materials (2012-ZD05).

■ REFERENCES

(1) Zou, Y.; Wan, M.; Sang, G.; Ye, M.; Li, Y. *Adv. Funct. Mater.* **2008**, *18*, 2724−2732.
(2) Tang, Y.; He, F.; Yu, M.; Feng, F.; An, L.; Sun, H.; Wang, S.; Li, Y.; Zhu, D. *Macromol. Rapid Commun.* **2006**, *27*, 389−392.
(3) Fan, L.; Jones, W. E., Jr. *J. Am. Chem. Soc.* **2006**, *128*, 6784−6785.
(4) Bao, B.; Yuwen, L.; Zhan, X.; Wang, L. *J. Polym. Sci., Polym. Chem.* **2010**, *48*, 3431−3439.
(5) Kim, I.; Bunz, U. H. F. *J. Am. Chem. Soc.* **2006**, *128*, 2818−2819.
(6) Zhou, X.; Yan, J.; Pei, J. *Macromolecules* **2004**, *37*, 7078−7080.
(7) Tong, H.; Wang, L.; Jing, X.; Wang, F. *Macromolecules* **2002**, *35*, 7169−7171.
(8) Kim, J.; McQuade, D. T.; McHugh, S. K.; Swager, T. M. *Angew. Chem., Int. Ed.* **2000**, *39*, 3868−3872.
(9) Ding, A.; Pei, J.; Yu, W.; Lai, Y.; Huang, W. *Thin Solid Films* **2002**, *417*, 198−201.
(10) Callan, J. F.; Prasanna de Silva, A.; Magri, D. C. *Tetrahedron* **2005**, *61*, 8551−8588.
(11) Haupt, K.; Mosbach, K. *Chem. Rev.* **2000**, *100*, 2495−2504.
(12) Vanden Bout, D. A.; Yip, W.; Hu, D.; Fu, D.; Swager, T. M.; Barbara, P. F. *Science* **1997**, *277*, 1074−1077.
(13) Lv, W.; Li, N.; Li, Y.; Li, Y.; Xia, A. *J. Am. Chem. Soc.* **2006**, *128*, 10281−10287.
(14) Ebihara, Y.; Vacha, M. *J. Phys. Chem. B* **2008**, *112*, 12575−12578.
(15) Kim, I.; Dunkhorst, A.; Bunz, U. H. F. *Langmuir* **2005**, *21*, 7985−7989.
(16) Feng, F.; He, F.; An, L.; Wang, S.; Li, Y.; Zhu, D. *Adv. Mater.* **2008**, *20*, 2959−2964.
(17) Wu, C.; Szymanski, C.; Cain, Z.; McNeill, J. *J. Am. Chem. Soc.* **2007**, *129*, 12904−12905.
(18) Tuncel, D.; Demir, H. V. *Nanoscale* **2010**, *2*, 484−494.
(19) Zheng, C.; Xu, X.; He, F.; Li, L.; Wu, B.; Yu, G.; Liu, Y. *Langmuir* **2010**, *26*, 16730−16736.
(20) Wang, D.; Zhang, J.; Luo, Q.; Li, X.; Duan, Y.; An, J. *J. Hazard. Mater.* **2009**, *169*, 546−550.
(21) Feng, X.; Yang, G.; Liu, L.; Lv, F.; Yang, Q.; Wang, S. *Adv. Mater.* **2012**, *24*, 637−641.
(22) Feng, X.; Lv, F.; Liu, L.; Tang, H.; Xing, C.; Yang, Q.; Wang, S. *ASC Appl. Mater. Interfaces* **2010**, *2*, 2429−2435.
(23) Fernando, L. P.; Kandel, P. K.; Yu, J.; McNeill, J.; Ackroyd, P. C.; Christensen, K. A. *Biomacromolecules* **2010**, *11*, 2675−2682.
(24) Howes, P.; Green, M.; Levitt, J.; Suhling, K.; Hughes, M. *J. Am. Chem. Soc.* **2010**, *132*, 3989−3996.
(25) Zhao, X.; Tapec-Dytioco, R.; Tan, W. *J. Am. Chem. Soc.* **2003**, *125*, 11474−11475.
(26) Zhao, X.; Hilliard, L. R.; Mechery, S. J.; Wang, Y.; Bagwe, R. P.; Jin, S.; Tan, W. *Proc. Natl. Acad. Sci. U.S.A.* **2004**, *101*, 15027−15032.
(27) Wang, J.; Xu, X.; Zhao, Y.; Zheng, C.; Li, L. *J. Mater. Chem.* **2011**, *21*, 18696−18703.
(28) Xu, X.; Chen, S.; Li, L.; Yu, G.; Di, C.; Liu, Y. *J. Mater. Chem.* **2008**, *18*, 2555−2561.
(29) Sonar, P.; Soh, M. S.; Cheng, Y. H.; Henssler, J. T.; Sellinger, A. *Org. Lett.* **2010**, *12*, 3292−3295.
(30) Chen, Y.; Lin, L.; Lu, C.; Lin, F.; Huang, Z.; Lin, H.; Wang, P.; Liu, Y.; Wong, K.; Wen, J.; Miller, D. J.; Darling, S. B. *J. Am. Chem. Soc.* **2012**, *134*, 13616−13623.
(31) Padhi, A. K.; Nanjundaswamy, K. S.; Goodenough, J. B. *J. Electrochem. Soc.* **1997**, *144*, 1188−1194.
(32) Padhi, A. K.; Nanjundaswamy, K. S.; Masquelier, C.; Okada, S.; Goodenough, J. B. *J. Electrochem. Soc.* **1997**, *144*, 1609−1613.
(33) Arnold, G.; Garche, J.; Hemmer, R.; Ströbele, S.; Vogler, C.; Wohlfahrt-Mehrens, M. *J. Power Sources* **2003**, *119*, 247−251.
(34) Delacourt, C.; Laffont, L.; Bouchet, R.; Wurm, C.; Leriche, J. B.; Morcrette, M.; Tarascon, J. M.; Masquelier, C. *J. Electrochem. Soc.* **2005**, *152*, A913−A921.
(35) Tang, K.; Sun, J.; Yu, X.; Li, H.; Huang, X. *Electrochim. Acta* **2009**, *54*, 6565−6569.
(36) Yuan, L.; Wang, Z.; Zhang, W.; Hu, X.; Chen, J.; Huang, Y.; Goodenough, J. B. *Energy Environ. Sci.* **2011**, *4*, 269−284.
(37) Doherty, C. M.; Caruso, R. A.; Drummond, C. J. *Energy Environ. Sci.* **2010**, *3*, 813−823.
(38) Kim, C. W.; Park, J. S.; Lee, K. S. *J. Power Sources* **2006**, *163*, 144−150.
(39) Hirosea, K.; Honma, T.; Doi, Y.; Hinatsu, Y.; Komatsu, T. *Solid State Commun.* **2008**, *146*, 273−277.
(40) Karamanev, D. G.; Nikolov, L. N.; Mamatarkova, V. *Miner. Eng.* **2002**, *15*, 341−346.
(41) Stucki, J. W. *Soil Sci. Soc. Am. J.* **1981**, *45*, 638−641.
(42) Li, L.; He, F.; Wang, X.; Ma, N.; Li, L. *ACS Appl. Mater. Interfaces* **2012**, *4*, 4927−4933.
(43) Dong, L.; Wu, C.; Zeng, X.; Mu, L.; Xue, S.; Tao, Z.; Zhang, J.-X. *Sensor. Actuat. B* **2010**, *145*, 433−427.
(44) Bastian, R.; Weberling, R.; Palilla, F. *Anal. Chem.* **1953**, *25*, 284−288.
(45) Zhou, G.; Qian, G.; Ma, L.; Cheng, Y.; Xie, Z.; Wang, L.; Jing, X.; Wang, F. *Macromolecules* **2005**, *38*, 5416−5424.
(46) Sumner, J. P.; Kopelman, R. *Analyst* **2005**, *130*, 528−533.
(47) Ma, Y.; Luo, W.; Quinn, P. J.; Liu, Z.; Hider, R. C. *J. Med. Chem.* **2004**, *47*, 6349−6362.
(48) Wu, T.; Chen, Y. *J. Polym. Sci., Polym. Chem.* **2004**, *42*, 1272−1284.
(49) Prasanna de Silva, A.; Nimal Gunaratne, H. Q.; Gunnlaugsson, T.; Huxley, A. J. M.; McCoy, C. P.; Rademacher, J. T.; Rice, T. E. *Chem. Rev.* **1997**, *97*, 1515−1566.
(50) Liu, J.; Zheng, Q.; Yang, J.; Chen, C.; Huang, Z. *Tetrahedron Lett.* **2002**, *43*, 9209−9212.
(51) Tumambac, G. E.; Rosencrance, C. M.; Wolf, C. *Tetrahedron* **2004**, *60*, 11293−11297.
(52) Wang, Q.; Tan, C. *Anal. Chim. Acta* **2011**, *708*, 111−115.
(53) Rathinam, B.; Chien, C.; Chen, B.; Liu, J. *Tetrahedron* **2013**, *69*, 235−241.
(54) Ni, Y.; Huang, C.; Kokot, S. *Anal. Chim. Acta* **2007**, *599*, 209−218.
(55) Madrakian, T.; Siri, R. *Acta Chim. Slov.* **2011**, *58*, 288−294.
(56) Yan, W.; Ye, X.; Akhmedov, N. G.; Petersen, J. L.; Shi, X. *Org. Lett.* **2012**, *14*, 2358−2361.
(57) Chereddy, N. R.; Thennarasu, S.; Mandal, A. B. *Dalton Trans.* **2012**, *41*, 11753−11759.

(58) Na, J.; Kim, Y.; Park, W. H.; Lee, T. S. *J. Polym. Sci., Polym. Chem.* **2004**, *42*, 2444−2450.
(59) Wu, C.; Peng, H.; Jiang, Y.; McNeill, J. *J. Phys. Chem. B* **2006**, *110*, 14148−14154.
(60) Chen, J. J.; Chen, T. L.; Kim, B.; Poulsen, D. A.; Mynar, J. L.; Fréchet, J. M. J.; Ma, B. *ACS Appl. Mater. Interfaces* **2010**, *2*, 2679−2686.
(61) Bomben, P. G.; Grodon, T. J.; Schott, E.; Berlinguette, C. P. *Angew. Chem., Int. Ed.* **2011**, *123*, 10870−10873.
(62) Haasnoot, J. G. *Coordin. Chem. Rev.* **2000**, *200*−*202*, 131−185.
(63) Liu, K.; Shi, W.; Cheng, P. *Dalton Trans.* **2011**, *40*, 8475−8490.
(64) Liu, Z. D.; Hider, R. C. *Med. Res. Rev.* **2002**, *22*, 26−64.
(65) Kim, I.; Phillips, R.; Bunz, U. H. F. *Macromolecules* **2007**, *40*, 814−817.